

Received November 11, 2019, accepted December 1, 2019, date of publication December 5, 2019,  
date of current version December 23, 2019.

Digital Object Identifier 10.1109/ACCESS.2019.2957753

# Indoor Smartphone Localization: A Hybrid WiFi RTT-RSS Ranging Approach

GUANGYI GUO<sup>ID</sup>, RUIZHI CHEN<sup>ID</sup>, FENG YE<sup>ID</sup>, XUESHENG PENG<sup>ID</sup>, ZUOYA LIU<sup>ID</sup>,  
AND YUANJIN PAN<sup>ID</sup>

State Key Laboratory of Information Engineering in Surveying, Mapping and Remote Sensing (LIESMARS), Wuhan University, Wuhan 430079, China

Corresponding author: Ruizhi Chen (ruizhi.chen@whu.edu.cn)

This work was supported in part by the National Key Research and Development Program of China under Grant 2016YFB0502200 and Grant 2016YFB0502201, and in part by the NSFC under Grant 91638203.

**ABSTRACT** Real-time locating and tracking Technology plays a significant role in location-based IoT applications. With the extensive installation of WiFi access points, the WiFi based indoor positioning approach has become one of the most widely used location technologies. However, due to the limitations of wireless signals, the classic WiFi-based method has become labor-intensive. Recently, the WiFi-based two-way ranging approach was introduced into the 802.11-REVmc2 protocol, which is built on a new packet type known as fine timing measurement (FTM) frame. In this work, we introduce the round-trip time measurement with clock skew and analyze the distribution of the round trip time (RTT) ranging error. A calibration method is presented to eliminate the RTT range offset at the transmitter end. We also develop an integrated ranging algorithm based on the WiFi round trip time range and received signal strength to enhance the scalability and robustness of the positioning system. The experimental results demonstrate that the proposed fusion method achieves remarkable improvement in scalability and precision in both static and dynamic tests, including outdoor and indoor environments. Compared with the classic fingerprinting approach, the performance of the system is remarkably improved, and achieves an average positioning accuracy of 1.435 m with an update rate of every 0.19 s.

**INDEX TERMS** Indoor localization, smartphone, WiFi fine time measurement (FTMs), round trip time (RTT), received signal strength (RSS), Kalman filter.

## I. INTRODUCTION

With billions of units in everyday use throughout the world, the smartphone has become a highly popular personal communication, ubiquitous computing, and entertainment platform. Many free and handy location-based applications offer great convenience for users in their daily lives. As the foundation of location-based services (LBS), accurate position information in the outdoors can be obtained from the Global Navigation Satellite System (GNSS). It is also true that a strong demand exists for a localization capability that can operate in buildings, both for individual users and Internet of Things (IoT) applications. As a high-interest research topic in academic and industrial field, real-time locating and tracking technology (RTLTT) has attracted the attention of many scholars who devote time and study to this area and are

The associate editor coordinating the review of this manuscript and approving it for publication was Rui-Jun Yan<sup>ID</sup>.

expected to play a pivotal role in the upcoming era of artificial intelligence (AI).

The current smartphone-based RTLTT can be divided into three categories: radio frequency (RF)-based methods, sensor-based methods and data fusion methods. The RF-based methods rely on wireless communication signals to locate and track the smartphone, including cellular [1]–[4], Wi-Fi [5]–[22], Bluetooth Low Energy (BLE) [23]–[26], Radio Frequency Identification (RFID) [27]–[29]. These approaches are based on different observations such as signal coverage, received signal strength (RSS), range (via time of arrival or round-trip time), range difference (via time difference of arrival) and direction (via angle of arrival). The sensor-based methods use smartphone built-in sensors to estimate the absolute or relative position. For example, the inertial navigation system (INS) [28], [30], [31] and pedestrian dead reckoning (PDR) [32]–[35] algorithms use measurements from the accelerometer, gyroscope,

magnetometer and barometer to estimate the relative displacement of the target. Magnetic matching (MM) methods [36]–[41] use the intense magnetic field interference and anomalies caused by the metal structure of the building to estimate the locations. Speaker/microphone-based ultrasonic (US) location systems [42]–[44] rely on the time of flight (TOF) or time difference of arrival (TDOA) measurements of US signal, which enabling centimeter- or decimeter-level location accuracy. Visual positioning systems [45]–[47] locate a camera by matching a captured image with a previously geo-referenced image database or 3D models. Because each RTLT has advantages and limitations, multi-sensor fusion methods [28], [48]–[53] are used to leverage the best features of each type of location-dependent observation and have become mainstream methods for indoor pedestrian localization. However, due to the complexity of the indoor environment and channel circumstances, as well as the unpredictability of user behavior, no one ubiquitous solution exists for indoor positioning similar to that of GNSS.

Recently, the WiFi-based two way ranging (TWR) approach found its way into the 802.11-REVmc2 protocol [54], which is built around a new packet type called a fine timing measurement (FTM) frame. Compared with TOA and TDOA, one of the most significant benefits of the RTT technique is that no clock synchronization is needed between the transmitter and receiver, which reduces the complexity and remarkably enhances the reliability of the indoor positioning system. Additionally, under the assumption that the clocks run at the same rate on the transmitter and receiver, the RTT ranging error and range between the two devices are nearly independent. Although the standardized FTM protocol can offer high-resolution ranging measurement and a high update rate compared with classic fingerprinting methods, the RTT range still encounters the following limitations:

- Similar to other wireless signals, RTT measurement also suffers from reflection, fading and shadowing in indoor environments.
- Due to the presence of phase noise, the clock cannot operate at an absolutely stable and accurate speed, which results in time measurement error at both the transmitter and receiver.
- The differences in the chipset hardware and firmware of WLAN cards at the transmitter end result in different processing time delays, which should not be included in the RTT measurement.
- As a point-to-point, single-user protocol, the FTM protocol is limited to concurrent processing capacity [55]. An AP cannot simultaneously respond to large numbers of FTM requests.

In this work, we aim to develop an integrated ranging algorithm based on the WiFi round trip time range and received signal strength to enhance the scalability and robustness of the positioning system. The architecture of the proposed positioning system on a smartphone is illustrated in FIGURE 1. Because of the presence of phase noise, the clock cannot operate at an absolutely stable and accurate speed. Therefore,

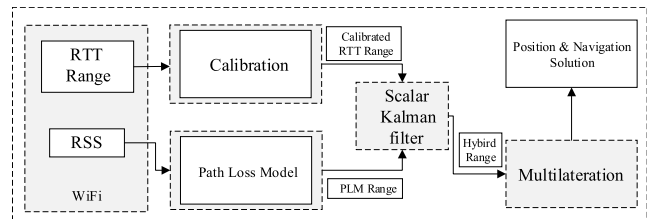


**FIGURE 1.** Scheme of positioning system.

the first task is to analyze the time surveying error caused by the clock skew in the RTT time measurement. Using a clock model, we also analyze the distribution of the RTT ranging error, which can be modeled as a Gaussian random process with zero mean and variance  $\sigma^2$ . Additionally, although the fine timing measurement frame is standardized in the 802.11-REVmc2 protocol, the differences in the network-card hardware and firmware results in processing delay [56], [57], which should not be counted in the RTT measurement. The RTT range offset caused by this delay in a transmitter is calibrated to further improve the accuracy of the RTT range. Finally, to address the limitation of RTT ranging, a scalar Kalman filter [58] is presented for fusion of the calibrated RTT range and RSS. Relying on the three remarkable characteristics of the Kalman filter, i.e., data filtering, smoothing and prediction, the proposed ranging method shows remarkable improvement in scalability and precision in both static and dynamic tests. The position accuracy, robustness and update rate of the system are notably improved in the real indoor environment, particularly compared with those of classic fingerprinting approach. Furthermore, the proposed method can complement the availability of the positioning system when a FTM request is denied.

In summary, the major contributions of this paper are listed as follows:

- We introduce round-trip time measurement with clock skew and analyze the distribution of the RTT ranging error which can be modeled as a Gaussian random process with zero mean and variance  $\sigma^2$ .
- Proceeding from the differences in transmitter hardware, we analyze the range offset caused by processing delay. A calibration approach is proposed to further improve the accuracy of the RTT range.
- The proposed ranging method shows remarkable improvement in scalability and precision in both static and dynamic tests, including outdoor and indoor environments.
- The position accuracy, robustness and update rate of the system are significantly improved in the real indoor environment, particularly compared with those of classic fingerprinting approach.

The remainder of this paper is organized as follows: Related works are summarized in Section II. Section III analyses the Wi-Fi signal observation in this paper, and Section IV describes the proposed integrated strategy of RTT range and RSS for indoor localization. Section V discusses the experiments and results. Section VI and VII provide a discussion

and conclusion of the whole work, respectively, and give suggestions for future research.

## II. RELATED WORKS

### A. INDOOR POSITIONING TECHNOLOGIES BASED ON WIFI

The current WiFi based indoor positioning systems can be divided into two categories: fingerprinting and multilateration approaches.

#### 1) FINGERPRINTING-BASED APPROACH

As one of the popular approaches for indoor positioning, fingerprinting-based methods offer many advantages, i.e., they are easily realizable and infrastructure-free. For these approaches, the two steps of offline database-building and online location estimation are necessary. In offline database-building, time-series RSS [5]–[11] measurements or channel state information (CSI) [12]–[14] data are collected at the reference points to build the wireless fingerprinting database. In real time location estimation, the location is estimated by matching the real-time signal measurement with the previously built fingerprinting database.

RADAR [5] is the first RSS-based fingerprinting system that uses a K-nearest neighbor (KNN) algorithm to estimate the location indoors. A weighted K-nearest neighbor (WKNN) [6] algorithm and a feature scaling-based K-nearest neighbor (FS-KNN) [7] method are proposed to improve the accuracy of the classical KNN algorithm. Hu [8] proposed a self-adaptive weighted KNN algorithm in which adapts with the RSS observation. Furthermore, Horus [9] used a probabilistic method for indoor positioning with RSS observation. Bayesian approaches [10], [11] have been used to enhance the quality fingerprinting database via a large number of data samples. In addition, PhaseFi [12] uses a deep network instead of the fingerprinting database and estimates the location using a radial basis function (RBF)-based probabilistic method. FIFS [13] utilizes the weighted average CSI values over multiple antennas to improve the performance of RSS-based method for indoor fingerprinting. DeepFi [14] learns a large amount of CSI amplitude data from three antennas for indoor localization based on a deep network.

However, both RSS-based and CSI-based fingerprinting methods have certain drawbacks. Large numbers of samples are needed to build a fingerprinting database, which is time-consuming and labor-intensive. Worse still, the radio map always suffers from the changing indoor environment. To maintain the positioning accuracy, the database must be updated constantly, and differentiation of mobile terminals also influences the positioning accuracy both online and offline.

#### 2) TRILATERATION/MULTILATERATION APPROACHES

The trilateration method uses the geometric properties of triangles to estimate the target location [15]. These approaches rely on the ranges between the transmitter and receiver, and

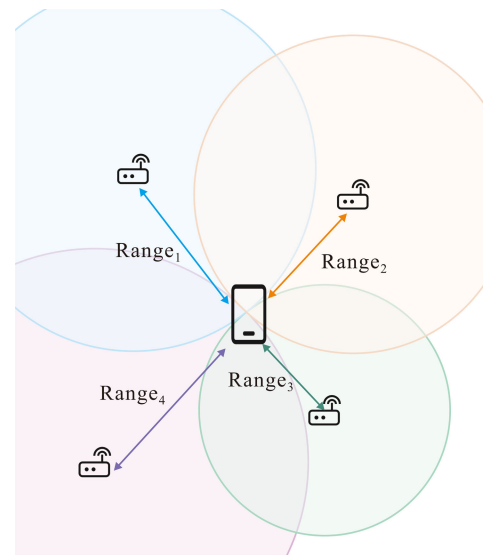


**FIGURE 2.** Multilateration, the process of converting ranges to a position.

need to survey the transmitter locations for position estimation. As shown in FIGURE 2, the 2D position of a smartphone  $X = (x, y)$  can be estimated from at least three ranges:

$$\begin{aligned} X &= (A^T A)^{-1} A^T L \\ A &= 2 \begin{bmatrix} x_1 - x_2 & y_1 - y_2 \\ \vdots & \vdots \\ x_1 - x_k & y_1 - y_k \end{bmatrix} \\ L &= \begin{bmatrix} Range_2^2 - Range_1^2 - (x_2^2 - x_1^2) - (y_2^2 - y_1^2) \\ \vdots \\ Range_k^2 - Range_1^2 - (x_k^2 - x_1^2) - (y_k^2 - y_1^2) \end{bmatrix} \quad (1) \end{aligned}$$

where  $(x_k, y_k)$  represents the location of  $AP_k$ , and  $Range_k$  is the measuring distance between the  $AP_k$  and the smartphone.

The RSS value attenuates rapidly with increasing range between the transmitter and receiver. Therefore, use of this rule can convert the RSS observation into a range. However, because the propagation channel is severe and the spatial topology is complex indoors, the attenuation rule is difficult to determine. In one-way ranging or TOA [16]–[18], [59], the separation between the transmitter and receiver is calculated using the travel time and speed of the signal. TDOA [19]–[21], uses the measurement of propagation time difference to calculate the range difference and estimate the location. Compared with the RSS-based ranging method, the time-based ranging system can obtain a higher accuracy and update rate. However, precision of time surveying and clock synchronization results in the limitation of system robustness and availability. With the increase in the size of the system, the complexity of the hardware and positioning algorithm also increase, which makes the system complex, expensive and fragile in dynamic indoor environments [48].

### B. FINE TIMING MEASUREMENT

The IEEE 802.11 working group approved amendment 802.11-REVmc<sup>2</sup> for the WiFi standard in 2016. A new

WiFi-based TWR approach was included in this amendment. In this technique, a smartphone initiates the FTM process by sending an FTM request to an access point (AP). The AP and smartphone start to send the FTM message and wait for its acknowledgement packet while the transmission and reception timestamp of each are recorded. This protocol is a ping-pong approach that calculates the propagation time by measuring the time it takes for a packet to be sent from an AP to a mobile and back again [22]. The round-trip time (RTT) is estimated based on the transmission timestamp of the FTM message and the reception of its ACK. FIGURE 3 shows an example of one burst with 1 FTM message. The RTT is calculated for an FTM message as follows:

$$RTT = (t_4 - t_1) - (t_3 - t_2) \quad (2)$$

Thus, the distance between the AP and smartphone can be obtained as follows:

$$Range_{RTT} = \frac{RTT}{2} \cdot c \quad (3)$$

### III. ANALYSIS OF WIFI SIGNAL OBSERVATIONS

#### A. CLOCK MODELING

The combination of an oscillator and counter constitute a clock which is a device used to measure time. An oscillator is an electronic circuit designed to generate periodic signals, usually a sinusoidal waveform. An ideal oscillator generates a pure sine wave, but phase noise (a ubiquitous common noise that exists in oscillators in practice) means that the oscillator cannot produce a pure sine wave. Usually, the noise is similar to the oscillation frequency and cannot be removed from the oscillation signal. This noise is referred to as oscillator phase noise.

Phase noise is the frequency domain representation of rapid, short-term, random fluctuations in the phase of a waveform caused by time domain instabilities (“jitter”) [60]. In this section, phase noise in oscillators is modeled by jitter, which is an impulse that perturbs the oscillator. The response to the perturbation is and is given as shown:

$$\Delta v(t) = (1 + \alpha(t))v(t + \phi(t)/2\pi f_0) - v(t) \quad (4)$$

where  $v(t)$  is the oscillator output voltage without jitter,  $\alpha(t)$  represents the variation in amplitude,  $f_0$  and  $\phi(t)$  represent the center frequency and random jitter of the oscillator, respectively.

Considering the effect of phase noise on the oscillator in a very short time, we can linearize (4) to obtain the following

$$\Delta v(t) = \frac{dv(t)}{dt} \cdot \frac{\Delta \phi(t)}{2\pi f_0} \quad (5)$$

This equation demonstrates that jitter affects the oscillator frequency periodically [61], which leads to the random offset and drift in a clock.

Due to the presence of phase noise, a clock cannot work at an absolutely stable and accurate speed, a phenomenon known as clock drift. As an important vital cause of clock drift, phase noise is usually dominated by many factors (i.e.,

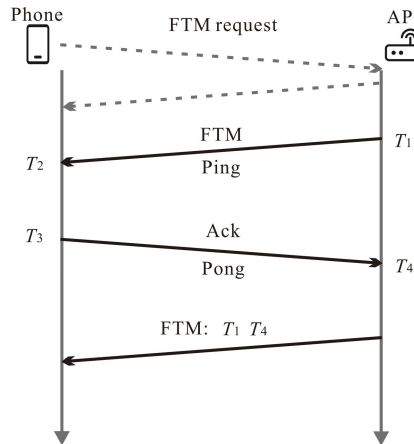


**FIGURE 3.** The 802.11mc2 fine timing measurement (FTM) protocol.

oscillator quality, pressure, humidity, use age). Therefore, for different clocks or even the same clock, the clock offset and drift rates are also not the same.

Clock offset is the difference between measurement of a clock and the ground truth, and the clock offset  $\theta(\tau)$  can be expressed as written:

$$\theta(\tau) = R(\tau) - \tau \quad (6)$$

where  $\tau$  is the actual time, and  $R(\tau)$  represents the time readings from a clock at  $\tau$ .

Clock skew  $v(\tau)$  is defined as the time difference with ground truth time  $\tau$ , which is the instantaneous drift of a clock.

$$v(\tau) = \frac{d\theta(\tau)}{d\tau} \approx \frac{d\theta(\tau + \Delta\tau) - d\theta(\tau)}{\Delta\tau} \quad (7)$$

The measurement  $T_t^m$  of a clock with skew and offset can be modeled as follows:

$$T_t^m = \tilde{T}_t + T_0 + \sum_{k=1}^t v_k \cdot \tau_k + \omega(t) \quad (8)$$

where  $\tilde{T}_t$  is the ground truth time,  $T_0$  represents the initial clock offset,  $v_k$  and  $\tau_k$  are the clock skew and sample period in the sample index  $k$ , respectively, and  $\omega(t)$  represents the random measurement noise.

#### B. ROUND TRIP TIME RANGING ESTIMATION

Figure 3 shows the principle of WiFi RTT, and the RTT measured by an ideal clock can be calculated using the equation (2). It is the nature of all clock systems to suffer from skew, drift and jitter. FIGURE 4 shows the RTT measured by clocks with clock skew and offset. This example uses a single 802.11mc<sup>2</sup>-supported AP and a smartphone. Both the AP and smartphone have initial timing offsets, which are denoted by  $T_0^T$  and  $T_0^R$ , respectively. In addition,  $v_k^T$  and  $v_k^R$  are the clock skew of the transmitter and receiver, respectively.

As mentioned in the previous section, the measurement of a clock with skew and offset can be modeled as shown in

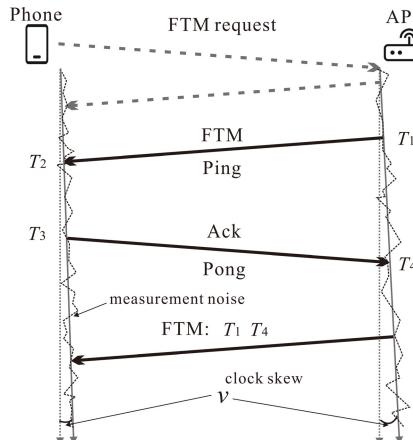


**FIGURE 4.** Round Trip Time (RTT) measurements with skewed clocks.

equation (8) and substituted into equation (2).

$$\begin{aligned} RTT_m &= \left( T_4^T - T_1^T \right) - \left( T_3^R - T_2^R \right) + T_p + 2 \cdot \omega_k^T + 2 \cdot \omega_k^R \\ &= (\tilde{T}_4 - \tilde{T}_1) - (\tilde{T}_3 - \tilde{T}_2) + T_p \\ &\quad + \left( \sum_{k=T_1}^{T_4} v_k^T \cdot \tau_k - \sum_{k=T_2}^{T_3} v_k^R \cdot \tau_k \right) + \omega_k \end{aligned} \quad (9)$$

where  $RTT_m$  is the round trip time measured by the clock,  $\tilde{T}$  represents the time measured by an ideal clock,  $T_p$  represents the MAC processing time delay,  $\omega_k^T$  is the AP clock measurement noise with zero mean and variance  $\sigma_T^2$ ,  $\omega_k^R$  is the smartphone clock measurement noise with zero mean and variance  $\sigma_R^2$ , and  $\omega_k$  represents the total clock measurement noise with zero mean and variance  $\sigma^2 = \sigma_T^2 + \sigma_R^2$ .

Many previous research studies [62], [63] have indicated that the time-varying clock skew caused by the phase noise in oscillator is a stochastic process. In this paper, we model the time-varying clock skew as a Gaussian random process with zero mean and variance  $\sigma^2$ . Therefore, equation (9) can be simplified as shown:

$$RTT_m = \tilde{RTT} + T_p + \omega_c \quad (10)$$

where  $\omega_c$  is the total clock measurement noise with zero mean and variance  $\sigma^2 = \sigma_T^2 + \sigma_R^2 + \sigma_{v_T}^2 + \sigma_{v_R}^2$ ,  $\sigma_{v_T}^2$ ,  $\sigma_{v_T}^2$  and  $\sigma_{v_R}^2$  are the clock skew variance of transmitter and receiver, respectively. Finally, the RTT range  $Range_{RTT}$  is given by the following:

$$\begin{aligned} d &= \frac{RTT_m - T_p}{2} \cdot c + \omega \\ &= d_m - d_{offset} + \omega \end{aligned} \quad (11)$$

where  $RTT_m$  and  $d_m$  represent the RTT measurement and RTT range measurement, respectively,  $d_{offset}$  is the range offset cause by MAC processing time delay, and  $\omega$  is the random measurement noise.

In this paper, we performed a survey on the RTT range data for fifty-four testing points, which measured the position with the total station in an indoor environment. In FIGURE 5, the orange colored bars represent the histogram of the raw RTT range error and give the best fit to the Gaussian

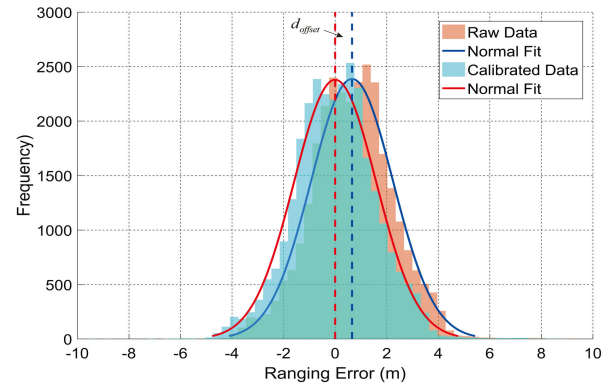


**FIGURE 5.** Comparison of range error histogram with a distribution fitting between raw RTT range and calibrated data.

distribution (blue curve) with a 0.656 m mean and 2.515 m<sup>2</sup> variance. The green bars represent the histogram of the calibrated data error, which removes range offset from the raw data. The red curve shows that calibrated data can be considered to obey a standard normal distribution with a zero mean and 2.515 m<sup>2</sup> variance.

Despite standardization according to the IEEE 802.11 protocol, the MAC processing time also depends on the chip set hardware and the firmware of the actual WLAN cards in use [64]. In other words, theoretically, no significant correlation exists between the range offset caused by the processing time delay and the distance between the transmitter and receiver. Therefore, the range offset must be fixed via transmitter calibration.

The collection of time-series RTT range readings at each reference point is used to calibrate the range offset  $d_{offset}$ , which is calculated as follows:

$$d_{offset} = \frac{1}{n} \sum_{k=1}^n (d_{m,k} - d) \quad (12)$$

where  $d_{m,k}$  is the range measurement at the reference point, for which the geometric range between transmitter is  $d$ , and  $n$  is the total sample number.

### C. WIRELESS RANGE ESTIMATION BASED ON RSS

The RSS (received signal strength), also referred to as RSSI (Received signal strength indicator), is a measurement of the power present in a received radio signal. Theoretically, the RSS value attenuates rapidly with the increase in range between the transmitter and receiver. The received power  $P_R$  at the receiver can be modeled as follows:

$$P_R \propto P_T \cdot \frac{G_t \cdot G_r}{4\pi d^n} \quad (13)$$

where  $P_T$  represents the transmitted power from the transmitter,  $G_t$  and  $G_r$  are the antenna gains of transmitter and receiver, respectively. Finally,  $d$  is the range between them.

The attenuation rule of the RSS vs. distances is known as the path loss model (PLM), which can be modeled by the

following expression [28], [48], [65], [66]:

$$RSS = RSS_0 - 10 \cdot n \cdot \log_{10}\left(\frac{d}{d_0}\right) + \omega \quad (14)$$

where  $RSS_0$  represents the RSS value observed at the reference point, the geometric range between transmitter is  $d_0$ .  $n$  is the path loss exponent, and  $\omega$  represents the Gaussian random noise with zero mean and variance  $\sigma_{RSS}^2$  and is used to describe the random process of shadowing [48], [67]. According to the equation (14), the RSS observation  $RSS(t)$  at time  $t$  obey the normal distribution with a  $RSS_0 - 10 \cdot n \cdot \log_{10}(d(t)/d_0)$  mean and  $\sigma_{RSS}^2(t)$  variance. Therefore, the probability density function (PDF) of  $RSS(t)$  is given as follows:

$$\begin{aligned} pdf(RSS) &= \frac{1}{\sqrt{2\pi}\sigma_{RSS}(t)} \\ &\exp\left(-\frac{\left(RSS(t) - \left(RSS_0 - 10 \cdot n \cdot \log_{10}\left(\frac{d}{d_0}\right)\right)\right)^2}{2\sigma_{RSS}^2(t)}\right) \end{aligned} \quad (15)$$

The distance  $d$  can be obtained by the maximum likelihood estimate (MLE) as follows:

$$\hat{d} = \arg \max_d pdf(RSS) \quad (16)$$

Because the logarithm function is a continuous and strictly increasing function over the range of the likelihood, the maximum of the likelihood necessarily maximizes its logarithm. To solve the maximum in a simple manner, we differentiate the log-likelihood function with respect to distance  $d$  to obtain the slope and set it equal to zero.

$$\begin{aligned} \frac{\partial \ln(pdf(RSS))}{\partial d} &= \frac{10 \cdot n \cdot d \cdot \left(RSS(t) - \left(RSS_0 - 10 \cdot n \cdot \log_{10}\left(\frac{d}{d_0}\right)\right)\right)}{\sigma_{RSS}^2(t) \cdot d_0^2 \cdot \ln 10} \\ &= 0 \end{aligned} \quad (17)$$

By simplifying equation (17), we write:

$$RSS(t) - \left(RSS_0 - 10 \cdot n \cdot \log_{10}\left(\frac{d}{d_0}\right)\right) = 0 \quad (18)$$

Consequently, the maximum likelihood estimator of the range  $d$  is given by the following:

$$d = d_0 \cdot 10^{\frac{RSS_0 - RSS}{10 \cdot n}} \quad (19)$$

The calibrated path loss model and the RSS samples in the reference points are shown in FIGURE 6.

#### IV. INTEGRATION STRATEGY

The Kalman filter [58], also known as line quadratic estimation (LQE), is a highly efficient recursive filter that estimates the state of a dynamic system from a series of inaccuracies and noise-containing measurements. When using the Kalman filter, it is no assumed that the error obeys the Gaussian

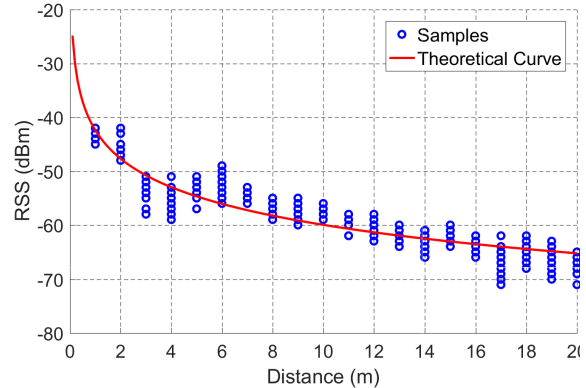


**FIGURE 6.** Theoretical path loss model. The solid red line corresponds to the PLM equation (14). The blue points represent the RSS samples in the reference points, which are used to calibrate the  $RSS_0$  and  $n$ .

distribution. However, the filter yields the exact conditional probability estimate in the special case that all errors are Gaussian [68]. The errors of WiFi RTT range and PLM range are modeled as a Gaussian random process in the previous section. Therefore, a scalar Kalman filter is designed to integrate these two range observations on a smartphone. The scalar state  $d_k$  in the KF at epoch  $k$  is expressed as follows:

$$x_k = [d_k] \quad (20)$$

The discrete linearization of the system model can be expressed as follows:

$$\begin{cases} x_{k|k-1} = A_k x_{k-1|k-1} + \omega_k \\ z_k = H_k x_{k|k-1} + v_k \end{cases} \quad (21)$$

where  $x_{k|k-1}$  is the predicted state,  $x_{k-1|k-1}$  is the previous state at epoch  $k-1$ , and  $z_k$  is the measurement vector. The transition matrix is  $A_k = I_{1 \times 1}$ , the design matrix is  $H_k = [1 \ 1]^T$ .  $\omega_k$  is the process noise with the covariance matrix  $Q_k = E(\omega_k \omega_k^T)$ , and  $v_k$  is the measurement noise with covariance matrix  $R_k = E(v_k v_k^T)$ . The observation vector is specified as shown

$$z_k = \begin{bmatrix} d_{RTT_k} - d_k^{offset} \\ RSS_0 - RSS^k \\ d_0 \cdot 10^{\frac{RSS_0 - RSS}{10 \cdot n}} \end{bmatrix} \quad (22)$$

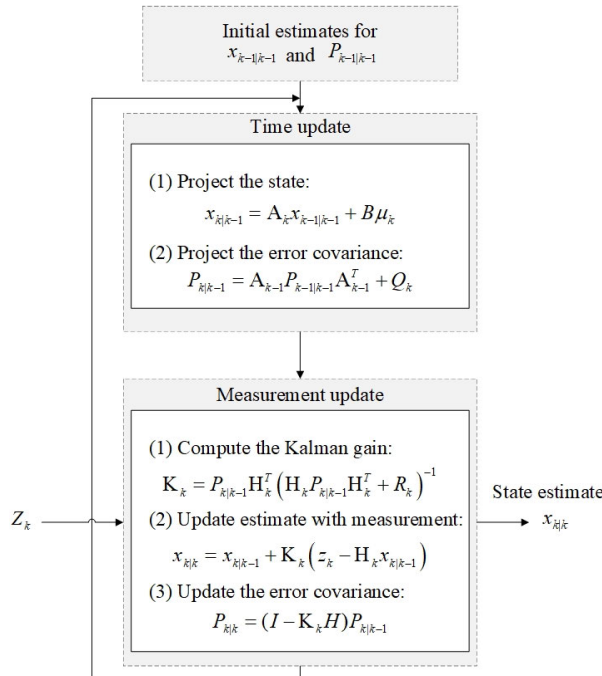
where  $d_{RTT_k}$  is the raw RTT range at epoch  $k$ ,  $d_k^{offset}$  is the calibration range offset,  $RSS_0$  represents the RSS value observed at the reference point, the geometric range between transmitter is  $d_0$ .  $n$  is the path loss exponent.

FIGURE 7 shows the algorithm of a Kalman filter designed to fuse the WiFi RTT range with the RSS observation for locating smartphone or IoT indoors.

#### V. EXPERIMENTAL EVALUATION

##### A. EXPERIMENTAL SETUP

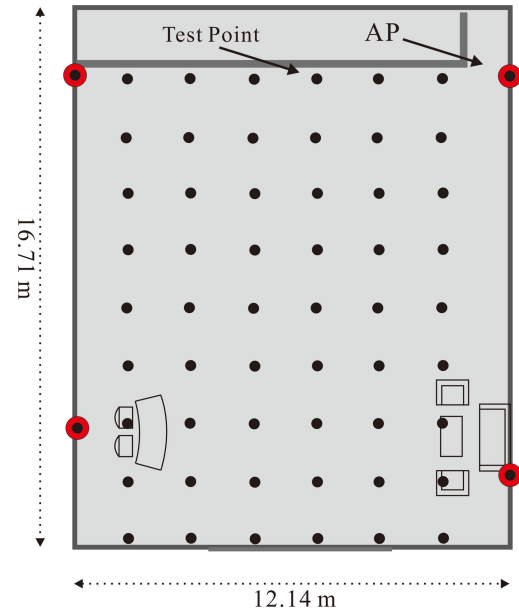
Three experiments were conducted to test the performance of the proposed algorithms. The first test consists of an evaluation of the accuracy of proposed ranging algorithm for static testing in outdoor and indoor environments. A total

**FIGURE 7.** Design of the Kalman filter.

of 20 reference points were set between the 802.11 mc protocol-supported AP and smartphones in an outdoor open field and corridor. The reference points for the measured distance ranged from one meter to twenty meters. Based on the Intel Dual Band Wireless-AC 8260 card and its open-source Linux driver, we built the WiFi APs for experiments. The WiFi data, including RTT range and RSS, were collected for one minute at each reference point using Google Pixel and Google Pixel 3 both with Android P. The ground truth of the range was measured using a tape measure.

The second test was designed to evaluate the accuracy of the proposed algorithm for dynamic testing in a corridor and in an outdoor environment. The testing trajectory was set between the 802.11 mc protocol-supported AP and smartphones in an outdoor open field and a corridor. The ground truth of the range was measured using the Leica Nova TS60 total station, which can automatically track a 360-degree prism and supply one observation every 0.15 s with 3-mm precision. The 360-degree was carried on the back of a participant who walked along the trajectory several times. The Google Pixel and Google Pixel 3 both with Android P were used to collect the RTT range and RSS in this experiment.

The third test is evaluated the accuracy of localization using the multilateration method and included a comparison with RSS based Finger-Printing method. This field test was conducted in the hall of Sirindhorn Research Center at Wuhan University. As shown in FIGURE 8, the field test area covers approximately 203 square meters. Four APs that support the 802.11 mc protocol were deployed in the hall for this test, and approximately fifty normal APs deployed in the building were used in the fingerprinting algorithm. Fifty-four testing

**FIGURE 8.** Experimental site.

points were set in the field test area and the positions were measured with Leica Nova TS60 total station. The WiFi data, including RTT range and RSS, were collected for 100 seconds at each testing point. Four smartphones were used in the experiment, namely, including Huawei Mate9, Huawei P9, Google Pixel and Google Pixel 3, were used in the experiment. The two Google smartphones were used to test the proposed algorithm. The other two Huawei smartphones were used to collect the RSS value for fingerprinting approach.

In the test, three indicators were established to evaluate and analyze the performance:

(1) Positioning accuracy (or positioning error) is the distance of positioning result deviation from the ground truth.

$$\delta_k = \|P_k - \tilde{P}_k\| \quad (23)$$

where  $\delta_k$  is the positioning error at epoch  $k$ ,  $P_k$  and  $\tilde{P}_k$  are the calculated position and ground truth position at epoch  $k$ , respectively.

(2) Robustness is defined as the percentage of the positioning result without outliers, with accuracy less than the threshold. In this test, 5 meters and 10 meters were selected as the threshold to evaluate the robustness of the method.

(3) Update rate is used to describe the time interval between the two positioning epochs.

## B. PERFORMANCE EVALUATION

### 1) STATIC RANGING PERFORMANCE EVALUATION IN OUTDOOR AND INDOOR ENVIRONMENTS

Figure 9 and Figure 10 illustrate the maximum and minimum values, lower and upper quartiles, median and outliers absolute ranging error of the raw RTT range data, calibrated data and proposed result at each one-meter reference point. The red line represents the median the of absolute ranging error, and the red points represent the outliers.

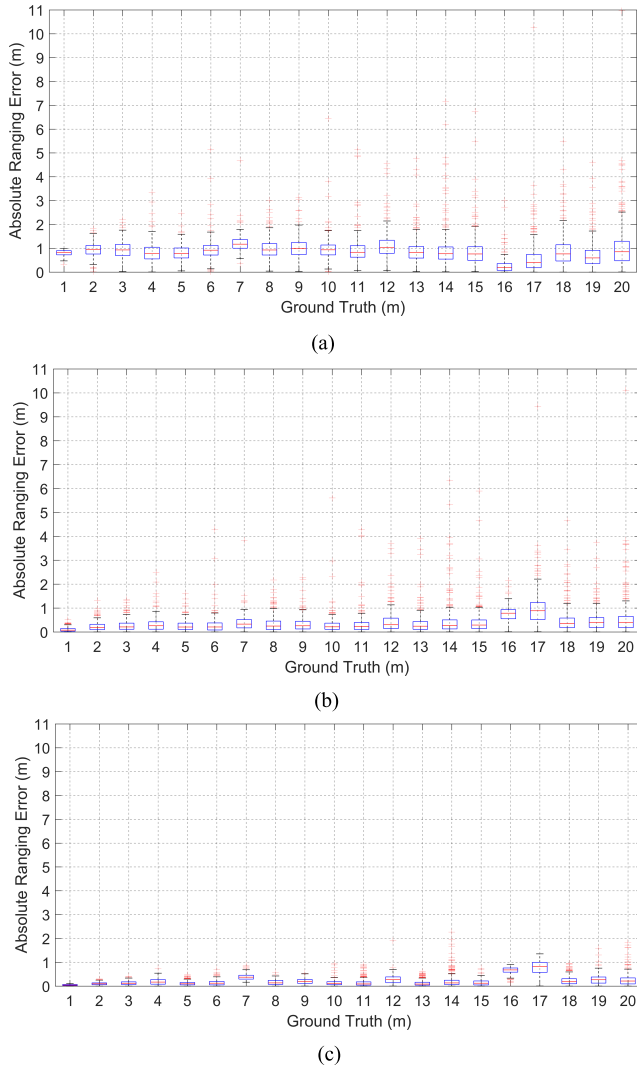


**FIGURE 9.** Comparison of the absolute ranging error in an outdoor environment: (a) Raw RTT range. (b) Calibrated range. (c) Fusion range.

As shown in Figure 9(a) and (b), the average absolute ranging errors of the raw data and calibrated data were 0.887 m, 0.414 m, respectively, in the outdoor open area. In Figure 10(a) and (b), the average absolute ranging error of the raw data and calibrated data were 0.896 m and 0.519 m, respectively, in the corridor. The absolute ranging errors of the calibrated data were improved by 53.32% (outdoor) and 42.08% (indoor) compared with the raw RTT range data in this test.

Figure 9(c) and Figure 10(c) show the performance of the proposed method with the highest accuracy and greatest robustness improvements by significant margins in both outdoor and indoor environments. In the outdoors, the proposed ranging errors were within (0 m, 3.391 m), the 25% and 75% errors were, respectively, 0.07 m and 0.309 m, and an error of variance  $0.058 \text{ m}^2$  was obtained. In the indoors, the proposed ranging error were within (0 m, 2.27 m), the 25% and 75% errors were, respectively, 0.175 m and 0.619 m, and error variance of  $0.058 \text{ m}^2$  was obtained.

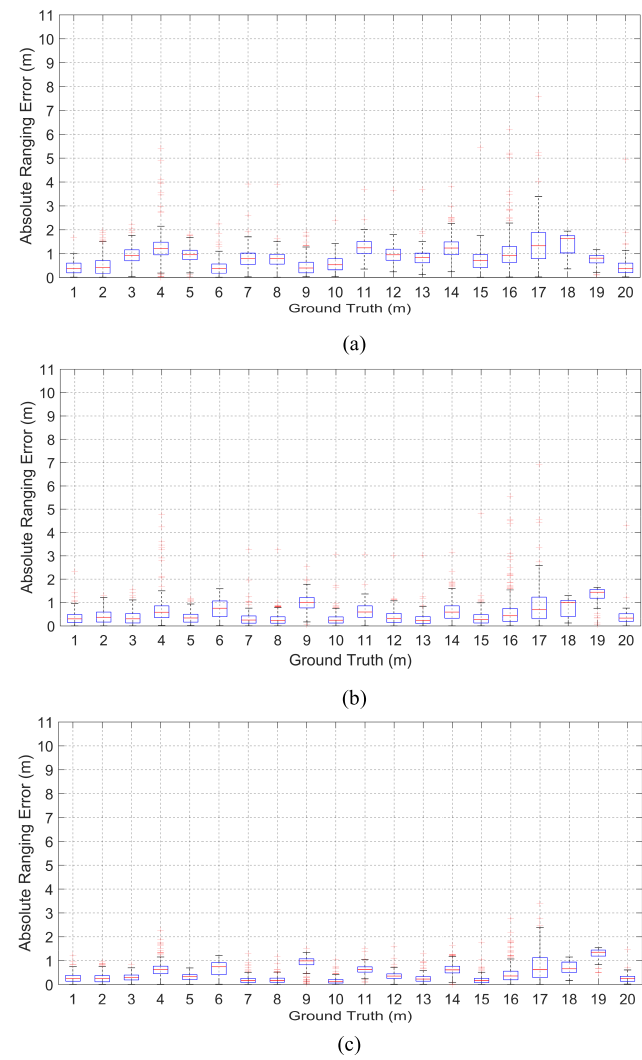


**FIGURE 10.** Comparison of the static ranging error in an indoor environment: (a) Raw RTT range. (b) Calibrated range. (c) Fusion range.

The overall ranging errors of the proposed method, in both outdoor and indoor environments, are less than the error of the raw RTT data and calibrated data. The absolute ranging cumulative error percentages of this test are depicted in Figure 11.

In Figure 11(a), the 50%, 95% and maximum errors of proposed method are 0.157 m, 0.771 m and 2.27 m, respectively, which are better than the corresponding values (0.828 m, 1.721 m and 10.96 m) obtained by the raw data and (0.286 m, 1.163 m and 10.11 m) obtained by the calibrated data in outdoor environment. For indoor environment, as shown in Figure 11(b), the 50%, 95% and maximum errors of proposed method are 0.347 m, 1.161 m and 3.391 m, respectively, which are better than the corresponding values (0.828 m, 1.838 m and 7.567 m) obtained by the raw data and (0.392 m, 1.363 m and 6.916 m) obtained by the calibrated data in the indoor environment. The statistics of absolute error, i.e., means, standard deviations, variance of the error, etc., were also listed and compared in Table 1.

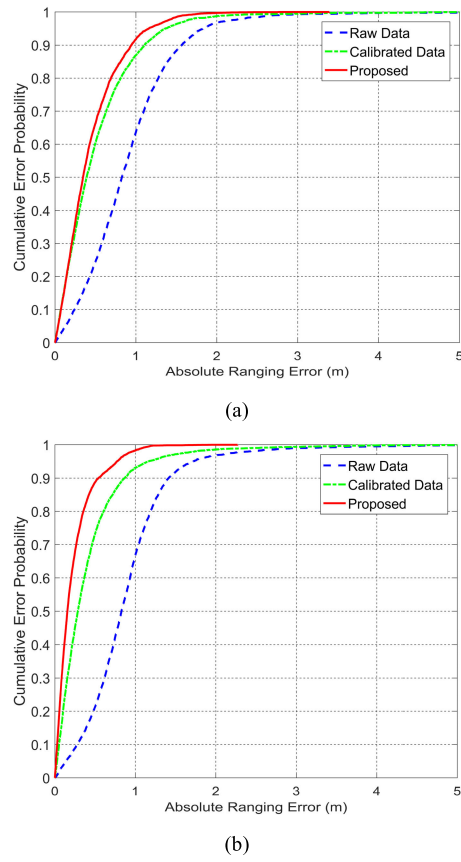


**FIGURE 11.** Cumulative error percentages in different cases: (a) Outdoor environment. (b) Indoor environment.

**TABLE 1.** The comparison of static ranging errors.

	<i>Stat.</i>	<i>Raw Data</i>	<i>Calibration Data</i>	<i>Proposed</i>
Outdoor	Mean (m)	0.887	0.414	0.233
	Std (m)	0.599	0.502	0.240
	Var (m <sup>2</sup> )	0.359	0.252	0.058
	Median (m)	0.828	0.286	0.157
	95th (m)	1.721	1.163	0.771
Indoor	Max (m)	10.960	10.110	2.270
	Min (m)	0.000	0.000	0.000
	Mean (m)	0.896	0.519	0.443
	Std (m)	0.587	0.498	0.366
	Var (m <sup>2</sup> )	0.344	0.248	0.134
	Median (m)	0.828	0.392	0.347
	95th (m)	1.838	1.363	1.161
	Max (m)	7.567	6.916	3.391
	Min (m)	0.003	0.001	0.000

The results indicate that the calibrated RTT range achieved a better level of accuracy than the raw RTT range in both outdoor and indoor environments. The RTT ranging offset

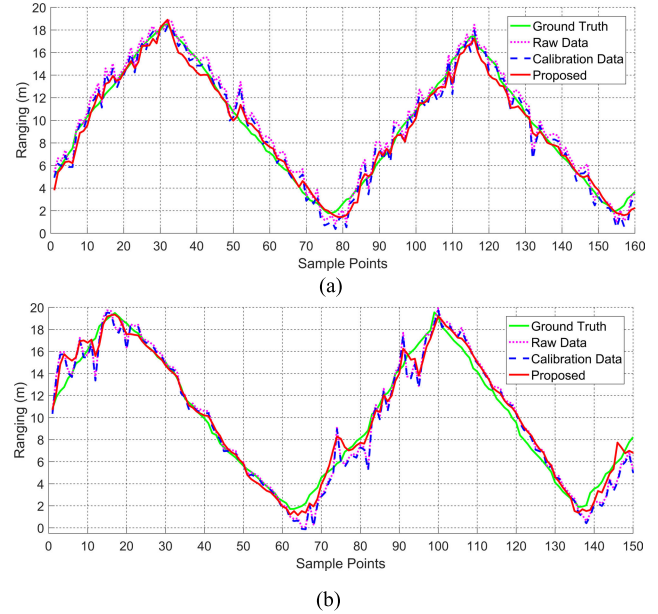


**FIGURE 12.** Comparison of dynamic ranging error in indoor (a) and outdoor (b) environments.

caused by the AP MAC processing time was removed to a certain degree by using calibrated compensation parameter. With the integration of WiFi RSS, the accuracy and precision of the ranging performance were improved, and the deviation of an outlier was reduced. Additionally, the overall ranging accuracy of the indoor tests was lower than that of the outdoor test due to the multipath effect, which results in ranging performance degradation. In the indoor environment, the transmitted signal is reflected and weakened by indoor objects (i.e., wall, door, bonsai and furniture) and reaches the receiver antenna by more than one path. These non-line of sight (NLOS) paths have different lengths resulting in different RTTs and RSS values, whereas the multipath effect is significantly reduced, in the outdoor open area.

## 2) DYNAMIC RANGING PERFORMANCE EVALUATION IN OUTDOOR AND INDOOR ENVIRONMENTS

With the integration of WiFi RSS, the proposed algorithm obtained the best accuracy and robust ranging performance in both outdoor and indoor environments, and resulted in much lower error than the raw RTT range data and calibrated data in Figure 12(a) and (b). The green line indicates the ground truth distance measured using the total station, and the pink dotted line and blue dotted line represent the raw RTT range and calibrated data, respectively. The red solid line is the proposed integration result.

In Figure 13(a), the 50%, 95% and maximum errors of the fusion method are 0.504 m, 1.386 m and 2.059 m in the outdoor open area, respectively, which are better than the corresponding values (0.717 m, 1.876 m, and 3.522 m) of raw RTT range data and those (0.634 m, 1.809 m, and 3.167 m) of the calibrated data. In addition, as shown in the Figure 13(b), the 50%, 95% and maximum errors of fusion

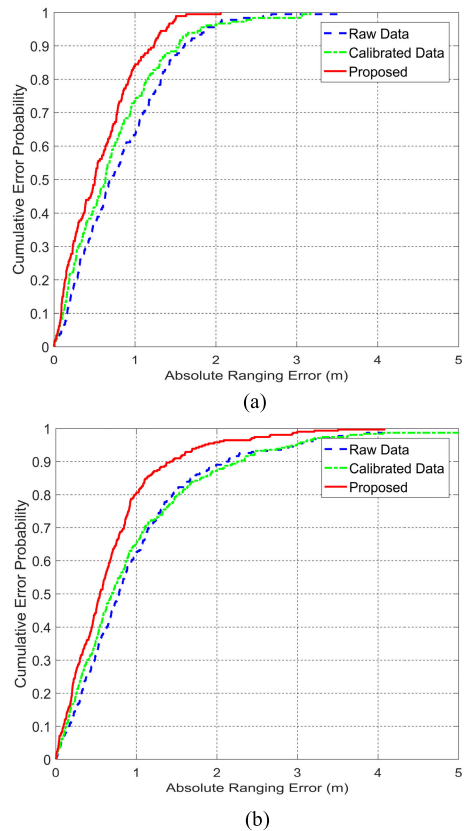


**FIGURE 13.** Cumulative error percentages in different cases: (a) Outdoor environment. (b) Indoor environment.

method are 0.586 m, 1.966 m and 2.998 m in the indoor corridor, respectively, which are better than the corresponding values (0.765 m, 2.798 m, and 4.061 m) of raw RTT range data and (0.699 m, 2.597 m, and 3.861 m) of the calibrated data.

As shown in Figure 13(a) and (b), the average absolute ranging errors of the raw data, calibrated data and proposed were 0.828 m, 0.733 m and 0.566 m in the outdoor open area, and 0.935 m, 0.910 m and 0.713 m in the corridor, respectively. The ranging error variance of the raw data, calibrated data and proposed method data were  $0.364 \text{ m}^2$ ,  $0.369 \text{ m}^2$  and  $0.184 \text{ m}^2$  in the outdoors, and  $0.641 \text{ m}^2$ ,  $0.687 \text{ m}^2$  and  $0.368 \text{ m}^2$  in the indoor, respectively. Compared with raw RTT ranging data, the absolute ranging errors were improved by 31.64% (outdoor) and 23.74% (indoor), and the variance were improved by 49.45% (outdoor) and 42.59% (indoor). The details of these tests are listed and compared in Table 2.

In this dynamic ranging test, the proposed method still achieved the highest precision and robustness both in outdoor and indoor environment. The overall accuracy of the ranging result in the outdoor open area still better than result obtained in the corridor. Because of both the RTT measurement and the RSS value, in indoor environment, suffered more multipath effect compared with in the open area. Furthermore, as shown in Figure 12(a) and (b), we clearly found that the measurement quality collected when facing the AP was superior to

**TABLE 2.** The comparison of dynamic ranging errors.

	Stat.	Raw Data	Calibration Data	Proposed
Outdoor	Mean (m)	0.828	0.733	0.566
	Std (m)	0.604	0.607	0.429
	Var ( $\text{m}^2$ )	0.364	0.369	0.184
	Median (m)	0.717	0.634	0.504
	95th (m)	1.876	1.809	1.386
	Max (m)	3.522	3.167	2.059
Indoor	Min (m)	0.006	0.002	0.000
	Mean (m)	0.935	0.910	0.713
	Std (m)	0.801	0.829	0.606
	Var ( $\text{m}^2$ )	0.641	0.687	0.368
	Median (m)	0.765	0.699	0.586
	95th (m)	2.798	2.597	1.966
	Max (m)	4.061	3.861	2.998
	Min (m)	0.004	0.002	0.005

that collected when facing away from the AP. During the dynamic ranging test, the participants walked towards the transmitter while holding the smartphone in front of their bodies and subsequently turned around and walked away from the transmitter. The rapid signal attenuation caused by body occlusion lead directly to this ranging performance drop. However, this phenomenon offers potential for NLOS detection to a certain extent. Moreover, compared with time measurement, RSS suffered more from this effect in principle, leading to a remarkable decrease in the precision of the pre-calibrated PLM.

### 3) POSITIONING PERFORMANCE EVALUATION IN OUTDOOR AND INDOOR ENVIRONMENTS

This section evaluates the performance of multilateration based on the RTT range and performs a comparison with RSS-based fingerprinting method. Figure 14 illustrates the four different positioning error distributions by interpolating the testing area using the positioning error of fifty-four testing points. The black solid points represent the testing points, and the positioning errors are labeled next to each point. Four red solid points indicate the 802.11 mc protocol-supported APs deployed in the testing region. The gradient of the color scale ranging from dark blue to bright yellow indicates the positioning error from low to high.

From the color changes, the fingerprinting method obtained the maximum percentage of the yellow region, whereas the proposed algorithm achieved the minimum percentage of the yellow region in this test. The overall trend showed increasing blue and decreasing yellow in the order of RSS-based fingerprinting, multilateration (raw RTT range data), multilateration (calibrated data), and multilateration (fusion range) methods.

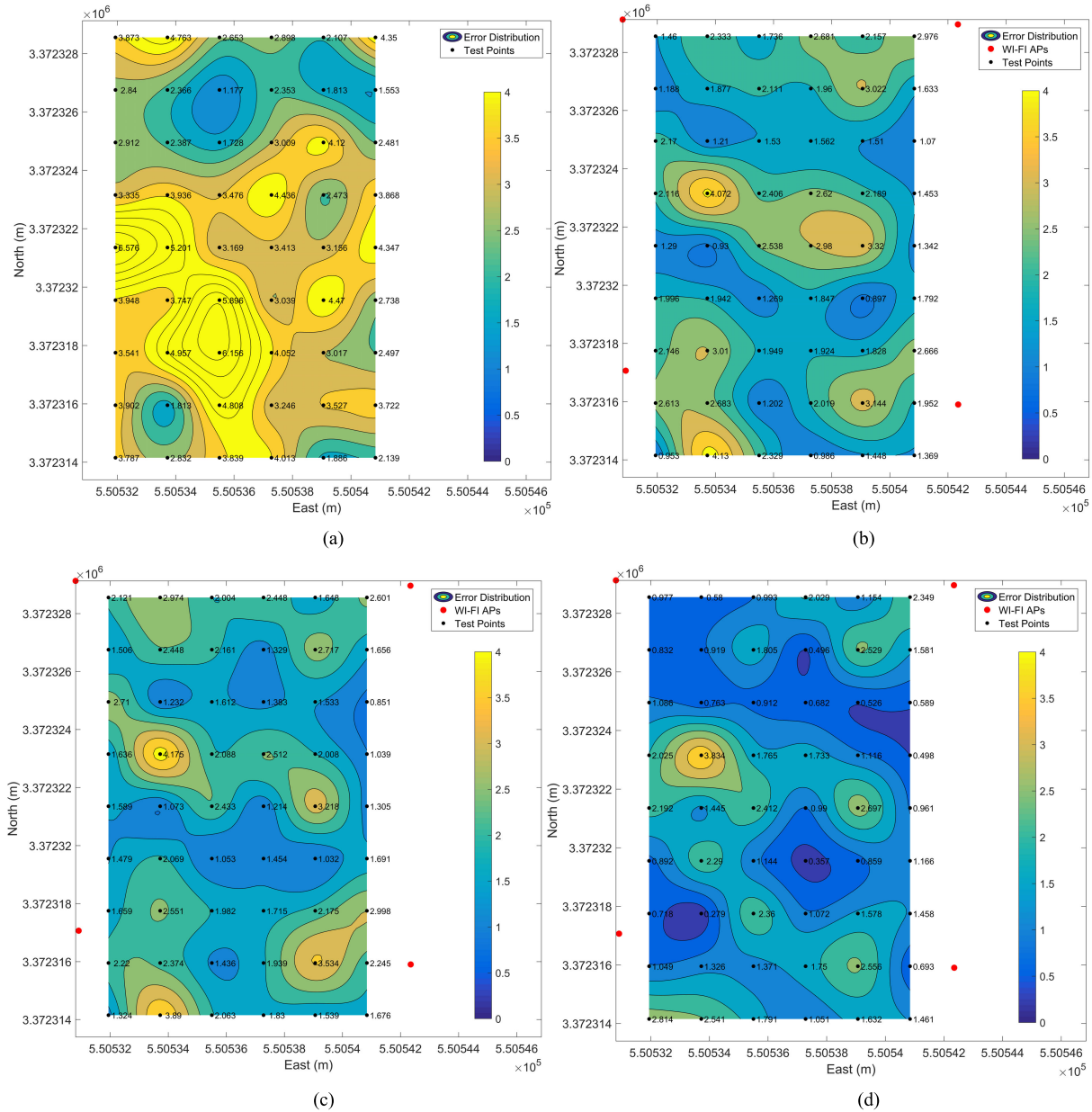


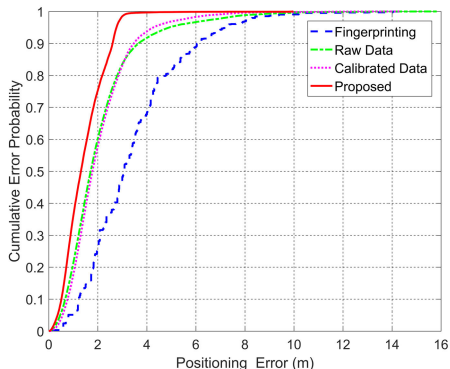
**FIGURE 14.** Positioning errors distribution in the testing region. (a) Fingerprint (b) Multilateration (raw RTT range). (c) Multilateration (calibrated RTT range). (d) Multilateration (proposed fusion range).

With the integration of WiFi RSS, the ranging error of the proposed algorithm was reduced and the ranging robustness was improved. Subsequently, the positioning accuracy was significantly enhanced. In particular, at the position close to each AP, the positioning accuracy was improved to a greater extent than elsewhere in the testing area. This observation is explained by the fact that the PLM based ranging method obtains better accuracy within a closer range of the transmitter. Therefore, the positioning accuracy of the proposed fusion approach is higher than that of the other method.

Figure 15 shows, the resulting cumulative distribution function for this experiment. The 50%, 95% and maximum positioning errors are 1.311 m, 2.761 m and 9.977 m, respectively,

for the multilateration with fusion ranging method in the testing region, which obtained the best result. The corresponding values of the RSS-based fingerprinting, multilateration with raw RTT range data and multilateration using calibrated data are (3.063 m, 7.351 m, and 14.6 m), (1.709 m, 4.918 m, and 15.825 m) and (1.779 m, 4.263 m, and 14.362 m), respectively. The means, standard deviations and variance of the error are also compared and listed in Table 4.

In this test, the positioning results from three indicators (i.e., positioning accuracy, robustness, update rate) among the four tests were compared and shown in Table 3. As shown, the multilateration with fusion RTT range achieved an average positioning error of 1.435 m, ten-meter robustness

**FIGURE 15.** Cumulative error percentages of localization errors.**TABLE 3.** The comparison of four aspects in this test.

Location	Accuracy	Robustness (10 m)	Robustness (5 m)	Update rate
source data	(m)	(10 m)	(5 m)	(s)
<i>Finger Printing</i>	3.412	99.07%	81.18%	2.52
<i>Raw Data</i>	2.063	99.64%	95.21%	0.23
<i>Calibrated Data</i>	2.042	99.84%	97.09%	0.23
<i>Proposed</i>	1.435	100%	99.81%	0.19

**TABLE 4.** The comparison of positioning errors.

Stat.	Finger Printing	Raw Data	Calibrated Data	Proposed
Mean (m)	3.412	2.063	2.042	1.435
Std (m)	1.993	1.555	1.286	0.819
Var (m <sup>2</sup> )	3.970	2.418	1.655	0.670
Median (m)	3.063	1.709	1.779	1.311
95th (m)	7.351	4.918	4.263	2.761
Max (m)	14.600	15.825	14.362	9.977
Min (m)	0.177	0.010	0.037	0.001

of 100%, five-meter robustness of 99.81% and 0.19 second update rate. The RSS based fingerprinting achieved an average positioning error of 3.412 m, ten-meters robustness of 99.07%, five-meters robustness of 81.18% and 2.52 seconds update rate. The corresponding values of fingerprinting, multilateration using raw RTT data and multilateration based calibrated RTT data are (3.412 m, 81.18%, and 2.52 seconds), (2.063 m, 95.21%, and 0.23 second) and (2.042 m, 97.09%, and 0.23 second), respectively.

The proposed fusion ranging approach obtains the best performance, improvement (57.98% in positioning accuracy, 18.63% in five-meter robustness), and reduction in positioning update rate more than 13 times that of the RSS-based fingerprinting method. The improvement (30.44% in positioning accuracy, 4.6% in five-meter robustness and 17.39%

in update rate) is compared with the result of multilateration using the raw RTT range data.

The positioning results indicated that the proposed ranging strategy not only promotes the location to be more robust and precise, also significantly reduces the update rate in a real indoor environment. This improvement is achieved through fusion of two different types of distance observation in WiFi signals with the designed Kalman filter, which is used to smooth and filter the data and to predict the range observation. Especially during the FTM request was denied result in the number of observation less than three, which was the minimum requirement of the multilateration. This is the reason why the positioning update rate of multilateration using the proposed ranging method was shorter than that using the raw RTT range data.

## VI. DISCUSSION

Overall, our studies established an indoor positioning solution on a consumer-grade smartphone. Evaluations of our methods in various environments shown that a hybrid WiFi RTT-RSS range can achieve a better level of accuracy than the raw RTT and RSS range in both outdoor and indoor environments. The results confirm that the position accuracy, robustness and update rate of the system were notably improved in the real indoor environment and achieved an average accuracy of 1.435 m with an update rate of every 0.19 s.

Compared with the most popular fingerprinting method, both WiFi RSS-based [5]–[11] and CSI-based [12]–[14] approaches, our approach do not need frequent and large numbers of samples to build and maintain the database. And due to the propagation channel is severe and the spatial topology is complex indoors, our algorithm can provide more accurate range and higher update rate both than RTT technique and PLM-based ranging method. Different with TOA [16]–[18] and TDOA [19]–[21], the positioning system based on RTT technique [54]–[57], [69] can obtain high reliability and the low system complexity. Compared with previous studies [22], [70], compensating the MAC processing delay caused by the differences of network-card hardware and firmware can improve the RTT ranging and positioning precision. Besides, the proposed hybrid ranging approach obviously reduces the influence of ranging request deny caused by limited concurrent processing power of the AP. To sum up, the positioning accuracy, robustness and the update rate can be significantly improved using the proposed method.

Although experiments have proven that our hybrid ranging strategy performed well on testing environment. Due to the influence of the complexity of the indoor spaces, channel circumstances and the unpredictability of user behavior, only wireless signal method is still challenging to achieve an accurate, effective, low cost and real time positioning solution. Our future work will focus on developing a pervasive integration platform to fuse wireless signal with MEMS sensors data.

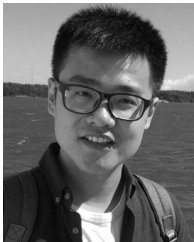
## VII. CONCLUSION

This paper introduced a smartphone positioning solution indoors by fusing WiFi RTT range and received signal strength to overcome the limitations of the WiFi round-trip time range. Field tests were conducted to verify the proposed ranging algorithm and the positioning solution in various environments and with different mobility. The performance of this fusion ranging method is reliable and can achieve average accuracies of 0.233 m (static) and 0.566 m (dynamic) in the outdoors, and 0.443 m (static) and 0.713 m (dynamic) indoors. The position accuracy, robustness and update rate of the system were notably improved in the real indoor environment and achieved an average accuracy of 1.435 m with an update rate of every 0.19 s. Our future work will focus on developing a pervasive integration platform to fuse wireless signal with MEMS sensors data to reduce the impacts of reflection, fading and shadowing of the wireless signals and achieve a more reliable locating solution for smartphones and IoT devices.

## REFERENCES

- [1] B. D. S. Lakmali and D. Dias, "Database correlation for GSM location in outdoor & indoor environments," in *Proc. 4th Int. Conf. Inf. Autom. Sustainab.*, Dec. 2008, pp. 42–47.
- [2] M. Koivisto, M. Costa, J. Werner, K. Heiska, J. Talvitie, K. Leppänen, V. Koivunen, and M. Valkama, "Joint device positioning and clock synchronization in 5G ultra-dense networks," *IEEE Trans. Wireless Commun.*, vol. 16, no. 5, pp. 2866–2881, May 2017.
- [3] R. S. Campos, "Evolution of positioning techniques in cellular networks—From 2G to 4G," *Wireless Commun. Mobile Comput.*, vol. 2017, 2017.
- [4] G. De Angelis, G. Baruffa, and S. Cacopardi, "GNSS/Cellular hybrid positioning system for mobile users in urban scenarios," *IEEE Trans. Intell. Transp. Syst.*, vol. 14, no. 1, pp. 313–321, Mar. 2013.
- [5] P. Bahl and V. N. Padmanabhan, "RADAR: An in-building RF-based user location and tracking system," in *Proc. 19th Annu. Joint Conf. IEEE Comput. Commun. Soc. (INFOCOM)*, vol. 2, Mar. 2000, pp. 775–784.
- [6] M. Brunato and R. Battiti, "Statistical learning theory for location fingerprinting in wireless LANs," *Comput. Netw.*, vol. 47, no. 6, pp. 825–845, 2005.
- [7] D. Li, B. Zhang, and C. Li, "A feature-scaling-based  $k$ -nearest neighbor algorithm for indoor positioning systems," *IEEE Internet Things J.*, vol. 3, no. 4, pp. 590–597, Aug. 2016.
- [8] J. Hu, D. Liu, Z. Yan, and H. Liu, "Experimental analysis on weight K-nearest neighbor indoor fingerprint positioning," *IEEE Internet Things J.*, vol. 6, no. 1, pp. 891–897, Feb. 2019.
- [9] M. Youssef and A. Agrawala, "The Horus WLAN location determination system," in *Proc. 3rd Int. Conf. Mobile Syst., Appl., Services*, 2005, pp. 205–218.
- [10] R. Berkvens, H. Peremans, and M. Weyn, "Conditional entropy and location error in indoor localization using probabilistic Wi-Fi fingerprinting," *Sensors*, vol. 16, no. 10, p. 1636, 2016.
- [11] K.-H. Kim and S.-B. Cho, "Modular Bayesian networks with low-power wearable sensors for recognizing eating activities," *Sensors*, vol. 17, no. 12, p. 2877, 2017.
- [12] X. Wang, L. Gao, and S. Mao, "CSI phase fingerprinting for indoor localization with a deep learning approach," *IEEE Internet Things J.*, vol. 3, no. 6, pp. 1113–1123, Dec. 2016.
- [13] J. Xiao, K. Wu, Y. Yi, and L. M. Ni, "FIFS: Fine-grained indoor fingerprinting system," in *Proc. 21st Int. Conf. Comput. Commun. Netw. (ICCCN)*, Jul. 2012, pp. 1–7.
- [14] X. Wang, L. Gao, S. Mao, and S. Pandey, "DeepFi: Deep learning for indoor fingerprinting using channel state information," in *Proc. IEEE Wireless Commun. Netw. Conf. (WCNC)*, Mar. 2015, pp. 1666–1671.
- [15] H. Liu, H. Darabi, P. Banerjee, and J. Liu, "Survey of wireless indoor positioning techniques and systems," *IEEE Trans. Syst., Man, Cybern. C, Appl. Rev.*, vol. 37, no. 6, pp. 1067–1080, Nov. 2007.
- [16] A. Gaber and A. Omar, "Sub-nanosecond accuracy of TDOA estimation using Matrix Pencil algorithms and IEEE 802.11," in *Proc. Int. Symp. Wireless Commun. Syst. (ISWCS)*, Aug. 2012, pp. 646–650.
- [17] A. Gholoobi and S. Stavrou, "A hybrid TDoA-ToA localization method," in *Proc. ICT*, May 2013, pp. 1–4.
- [18] S. König, M. Schmidt, and C. Hoene, "Precise time of flight measurements in IEEE 802.11 networks by cross-correlating the sampled signal with a continuous Barker code," in *Proc. 7th IEEE Int. Conf. Mobile Ad-Hoc Sensor Syst. (MASS)*, Nov. 2010, pp. 642–649.
- [19] Z. He, Y. Ma, and R. Tafazolli, "Improved high resolution TOA estimation for OFDM-WLAN based indoor ranging," *IEEE Wireless Commun. Lett.*, vol. 2, no. 2, pp. 163–166, Apr. 2013.
- [20] R. Exel, G. Gaderer, and P. Loschmidt, "Localisation of wireless LAN nodes using accurate TDoA measurements," in *Proc. IEEE Wireless Commun. Netw. Conf.*, Apr. 2010, pp. 1–6.
- [21] S. A. Napoleon, A. S. Omar, S. H. Elmaly, S. A. Khamis, and M. E. Nasr, "C5: Time difference of arrival by IEEE 802.11a, g based on practical estimation," in *Proc. 29th Nat. Radio Sci. Conf. (NRSC)*, Apr. 2012, pp. 185–190.
- [22] R. Want, W. Wang, and S. Chesnutt, "Accurate indoor location for the IoT," *Computer*, vol. 51, no. 8, pp. 66–70, 2018.
- [23] R. Faragher and R. Harle, "An analysis of the accuracy of Bluetooth low energy for indoor positioning applications," in *Proc. 27th Int. Tech. Meeting Satell. Division Inst. Navigat. (ION GNSS+)*, 2014, pp. 201–210.
- [24] R. Faragher and R. Harle, "Location fingerprinting with Bluetooth low energy beacons," *IEEE J. Sel. Areas Commun.*, vol. 33, no. 11, pp. 2418–2428, Nov. 2015.
- [25] L. Chen, L. Pei, H. Kuusniemi, Y. Chen, T. Kröger, and R. Chen, "Bayesian fusion for indoor positioning using Bluetooth fingerprints," *Wireless Pers. Commun.*, vol. 70, no. 4, pp. 1735–1745, 2013.
- [26] Y. Zhuang, J. Yang, Y. Li, L. Qi, and N. El-Sheimy, "Smartphone-based indoor localization with Bluetooth low energy beacons," *Sensors*, vol. 16, no. 5, p. 596, Apr. 2016.
- [27] L. M. Ni, Y. Liu, Y. C. Lau, and A. P. Patil, "LANDMARC: Indoor location sensing using active RFID," in *Proc. 1st IEEE Int. Conf. Pervasive Comput. Commun. (PerCom)*, Mar. 2003, pp. 407–415.
- [28] A. R. J. Ruiz, F. S. Granja, J. C. P. Honorato, and J. I. G. Rosas, "Accurate pedestrian indoor navigation by tightly coupling foot-mounted IMU and RFID measurements," *IEEE Trans. Instrum. Meas.*, vol. 61, no. 1, pp. 178–189, Jan. 2012.
- [29] A. Bekkali, H. Sanson, and M. Matsumoto, "RFID indoor positioning based on probabilistic RFID map and Kalman filtering," in *Proc. 3rd IEEE Int. Conf. Wireless Mobile Comput., Netw. Commun. (WiMob)*, Oct. 2007, p. 21.
- [30] A. R. Jiménez, F. Seco, J. C. Prieto, and J. Guevara, "Indoor pedestrian navigation using an INS/EKF framework for yaw drift reduction and a foot-mounted IMU," in *Proc. Workshop Positioning Navigat. Commun.*, Mar. 2010, pp. 135–143.
- [31] G. Retscher and Q. Fu, "Continuous indoor navigation with RFID and INS," in *Proc. IEEE/ION Position, Location Navigat. Symp.*, May 2010, pp. 102–112.
- [32] R. Chen, L. Pei, and Y. Chen, "A smart phone based PDR solution for indoor navigation," in *Proc. 24th Int. Tech. Meeting Satell. Division Inst. Navigat.*, Sep. 2011, pp. 1404–1408.
- [33] J. Kuang, X. Niu, and X. Chen, "Robust pedestrian dead reckoning based on MEMS-IMU for smartphones," *Sensors*, vol. 18, no. 5, p. 1391, 2018.
- [34] G. Guo, R. Chen, F. Ye, L. Chen, Y. Pan, M. Liu, and Z. Cao, "A pose awareness solution for estimating pedestrian walking speed," *Remote Sens.*, vol. 11, no. 1, p. 55, 2019.
- [35] A. R. Jimenez, F. Seco, C. Prieto, and J. Guevara, "A comparison of pedestrian dead-reckoning algorithms using a low-cost MEMS IMU," in *Proc. IEEE Int. Symp. Intell. Signal Process.*, Aug. 2009, pp. 37–42.
- [36] W. Storms, J. Shockley, and J. Raquet, "Magnetic field navigation in an indoor environment," in *Proc. Ubiquitous Positioning Indoor Navigat. Location Based Service*, Oct. 2010, pp. 1–10.
- [37] J. Chung, M. Donahoe, C. Schmandt, I.-J. Kim, P. Razavai, and M. Wiseman, "Indoor location sensing using geo-magnetism," in *Proc. 9th Int. Conf. Mobile Syst., Appl., Services*, 2011, pp. 141–154.
- [38] B. Gozick, K. P. Subbu, R. Dantu, and T. Maeshiro, "Magnetic maps for indoor navigation," *IEEE Trans. Instrum. Meas.*, vol. 60, no. 12, pp. 3883–3891, Dec. 2011.
- [39] G. De Angelis, A. De Angelis, A. Moschitta, and P. Carbone, "Comparison of measurement models for 3D magnetic localization and tracking," *Sensors*, vol. 17, no. 11, p. 2527, 2017.

- [40] G. De Angelis, A. De Angelis, V. Pasku, A. Moschitta, and P. Carbone, "An experimental system for tightly coupled integration of GPS and AC magnetic positioning," *IEEE Trans. Instrum. Meas.*, vol. 65, no. 5, pp. 1232–1241, May 2016.
- [41] V. Pasku, A. De Angelis, G. De Angelis, D. D. Arumugam, M. Dionigi, P. Carbone, A. Moschitta, and D. S. Ricketts, "Magnetic field-based positioning systems," *IEEE Commun. Surveys Tuts.*, vol. 19, no. 3, pp. 2003–2017, 3rd Quart., 2017.
- [42] F. Ijaz, H. K. Yang, A. W. Ahmad, and C. Lee, "Indoor positioning: A review of indoor ultrasonic positioning systems," in *Proc. 15th Int. Conf. Adv. Commun. Technol. (ICACT)*, Jan. 2013, pp. 1146–1150.
- [43] F. Höflinger, R. Zhang, J. Hoppe, A. Bannoura, L. M. Reindl, J. Wendeburg, M. Bührer, and C. Schindelhauer, "Acoustic self-calibrating system for indoor smartphone tracking (assist)," in *Proc. Int. Conf. Indoor Positioning Indoor Navigat. (IPIN)*, Nov. 2012, pp. 1–9.
- [44] K. Liu, X. Liu, and X. Li, "Guoguo: Enabling fine-grained smartphone localization via acoustic anchors," *IEEE Trans. Mobile Comput.*, vol. 15, no. 5, pp. 1144–1156, May 2016.
- [45] M. Werner, M. Kessel, and C. Marouane, "Indoor positioning using smartphone camera," in *Proc. Int. Conf. Indoor Positioning Indoor Navigat.*, Sep. 2011, pp. 1–6.
- [46] D. Van Opdenbosch, G. Schroth, R. Huitl, S. Hilsenbeck, A. Garcea, and E. Steinbach, "Camera-based indoor positioning using scalable streaming of compressed binary image signatures," in *Proc. IEEE Int. Conf. Image Process. (ICIP)*, Oct. 2014, pp. 2804–2808.
- [47] Y. Chen, R. Chen, M. Liu, A. Xiao, D. Wu, and S. Zhao, "Indoor visual positioning aided by CNN-based image retrieval: Training-free, 3D modeling-free," *Sensors*, vol. 18, no. 8, p. 2692, 2018.
- [48] Y. Zhuang, J. Yang, L. Qi, Y. Li, Y. Cao, and N. El-Sheimy, "A pervasive integration platform of low-cost MEMS sensors and wireless signals for indoor localization," *IEEE Internet Things J.*, vol. 5, no. 6, pp. 4616–4631, Dec. 2017.
- [49] L.-H. Chen, E. H.-K. Wu, M.-H. Jin, and G.-H. Chen, "Intelligent fusion of WiFi and inertial sensor-based positioning systems for indoor pedestrian navigation," *IEEE Sensors J.*, vol. 14, no. 11, pp. 4034–4042, Nov. 2014.
- [50] W. Xiao, W. Ni, and Y. K. Toh, "Integrated WiFi fingerprinting and inertial sensing for indoor positioning," in *Proc. Int. Conf. Indoor Positioning Indoor Navigat.*, Sep. 2011, pp. 1–6.
- [51] F. Evennou and F. Marx, "Advanced integration of WiFi and inertial navigation systems for indoor mobile positioning," *EURASIP J. Appl. Signal Process.*, vol. 2006, pp. 164–164, Jan. 2006.
- [52] U. Schatzberg, L. Banin, and Y. Amizur, "Enhanced WiFi ToF indoor positioning system with MEMS-based INS and pedometric information," in *Proc. IEEE/ION Position, Location Navigat. Symp.-PLANS*, May 2014, pp. 185–192.
- [53] C.-J. Sun, H.-Y. Kuo, and C. E. Lin, "A sensor based indoor mobile localization and navigation using unscented Kalman filter," in *Proc. IEEE/ION Position, Location Navigat. Symp.*, May 2010, pp. 327–331.
- [54] *IEEE Standard for Information Technology—Telecommunications and Information Exchange Between Systems Local and Metropolitan Area Networks—Specific Requirements—Part 11: Wireless LAN Medium Access Control (MAC) and Physical Layer (PHY) Specifications*, IEEE Standard 802.11, 2007.
- [55] L. Banin, O. Bar-Shalom, N. Dvorecki, and Y. Amizur, "High-accuracy indoor geolocation using collaborative time of arrival (CToA)," Santa Clara, CA, USA, Sep. 2017.
- [56] M. Ciurana, F. Barcelo-Arroyo, and F. Izquierdo, "A ranging method with IEEE 802.11 data frames for indoor localization," in *Proc. IEEE Wireless Commun. Netw. Conf.*, Mar. 2007, pp. 2092–2096.
- [57] A. Makki, A. Siddig, M. Saad, and C. Bleakley, "Survey of WiFi positioning using time-based techniques," *Comput. Netw.*, vol. 88, pp. 218–233, Sep. 2015.
- [58] R. E. Kalman, "A new approach to linear filtering and prediction problems," *J. Basic Eng.*, vol. 82, no. 1, pp. 35–45, 1960.
- [59] M. Ke, Y. Xu, A. Anpalagan, D. Liu, and Y. Zhang, "Distributed TOA-based positioning in wireless sensor networks: A potential game approach," *IEEE Commun. Lett.*, vol. 22, no. 2, pp. 316–319, Oct. 2018.
- [60] E. Rubiola, *Phase Noise and Frequency Stability in Oscillators*. Cambridge, U.K.: Cambridge Univ. Press, 2009.
- [61] J. Phillips and K. Kundert, "Noise in mixers, oscillators, samplers, and logic an introduction to cyclostationary noise," in *Proc. IEEE Custom Integr. Circuits Conf.*, May 2000, pp. 431–438.
- [62] B. R. Hamilton, X. Ma, Q. Zhao, and J. Xu, "ACES: Adaptive clock estimation and synchronization using Kalman filtering," in *Proc. 14th ACM Int. Conf. Mobile Comput. Netw.*, 2008, pp. 152–162.
- [63] D. Veitch, S. B. Korada, and A. Pásztor, "Robust synchronization of software clocks across the Internet," in *Proc. ACM SIGCOMM Conf. Internet Meas.*, 2004, pp. 219–232.
- [64] A. Günther and C. Hoene, "Measuring round trip times to determine the distance between WLAN nodes," in *NETWORKING 2005. Networking Technologies Services and Protocols; Performance of Computer and Communication Networks; Mobile and Wireless Communications Systems*. New York, NY, USA: Springer, 2005, pp. 768–779.
- [65] S. Mazuelas, A. Bahillo, R. M. Lorenzo, P. Fernandez, F. A. Lago, E. Garcia, J. Blas, and E. J. Abril, "Robust indoor positioning provided by real-time RSSI values in unmodified WLAN networks," *IEEE J. Sel. Topics Signal Process.*, vol. 3, no. 5, pp. 821–831, Oct. 2009.
- [66] J. Proakis, *Digital Communications*, 4th ed. New York, NY, USA: McGraw-Hill, 1983.
- [67] J. Salo, L. Vuokko, H. M. El-Sallabi, and P. Vainikainen, "An additive model as a physical basis for shadow fading," *IEEE Trans. Veh. Technol.*, vol. 56, no. 1, pp. 13–26, Jan. 2007.
- [68] G. Welch and G. Bishop, "An introduction to the Kalman filter," Univ. North Carolina, Chapel Hill, NC, USA, 2001.
- [69] *Wireless LAN Medium Access Control (MAC) and Physical Layer (PHY) Specifications*, IEEE Standard 802.5, 1997.
- [70] M. Ibrahim, H. Liu, M. Jawahar, V. Nguyen, M. Gruteser, R. Howard, B. Yu, and F. Bai, "Verification: Accuracy evaluation of WiFi fine time measurements on an open platform," in *Proc. 24th Annu. Int. Conf. Mobile Comput. Netw.*, 2018, pp. 417–427.



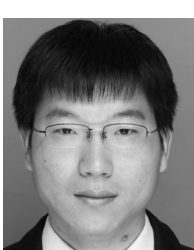
**GUANGYI GUO** received the B.S. and M.S. degrees in geographic information science from Hubei University, China, in 2012 and 2015, respectively. He is currently pursuing the Ph.D. degree in cartography and geographical information science, Wuhan University, Wuhan, China. His research interests include indoor positioning, machine learning, and the Internet of Things.



RUIZHI CHEN was an Endowed Chair Professor with Texas A&M University Corpus Christi, USA, the Head and a Professor of the Department of Navigation and Positioning, Finnish Geodetic Institute, Finland, and an Engineering Manager with Nokia, Finland. He is currently a Professor and the Director of the State Key Laboratory of Information Engineering in Surveying, Mapping and Remote Sensing, Wuhan University. He has published two books and more than 200 scientific articles. His current research interests include indoor positioning, satellite navigation, and location-based services.



FENG YE received the B.S. degree in automation and the M.S. degree in optical engineering from Huazhong University of Science and Technology, China, in 2014 and 2017, respectively. He is currently pursuing the Ph.D. degree in geodesy and survey engineering with Wuhan University, Wuhan, China. His research interests include indoor positioning, ubiquitous computing, machine learning, and the Internet of Things.



XUESHENG PENG received the B.S. degree in land resources management from Wuhan University, Wuhan, China, in 2014, and the M.S. degree in surveying and mapping engineering from Henan Polytechnic University, China, in 2017. He is currently pursuing the Ph.D. degree in geodesy and survey engineering with Wuhan University, Wuhan. His research interests include indoor positioning and the Internet of Things.



**ZUOYA LIU** received the B.S. degree in electronic information science and technology and the M.S. degree in electronic circuit and system from Central China Normal University, China, in 2012 and 2015, respectively. He is currently pursuing the Ph.D. degree in cartology and geographical information science with Wuhan University, Wuhan, China. His research interests include indoor positioning, navigation, machine learning, and the Internet of Things.



**YUANJIN PAN** was born in Jiangsu, China, in 1983. He received the Ph.D. degree in surveying and mapping engineering from Wuhan University. He has authored 15 articles in refereed journals and conferences. His research interests include indoor positioning, GNSS, and geodynamics of earth science.

• • •